Z. Phys. D 38, 59–64 (1996)

ZEITSCHRIFT
FÜR PHYSIK D

Photoionization of alkali metal clusters

Olaf Frank, Jan M. Rost

Fakultät für Physik, Universität Freiburg, Hermann-Herder-Strasse 3, D-79104 Freiburg, Germany

Received: 13 January 1996/Final version: 30 March 1996

Abstract. The photoionization cross section for spherical alkali metal clusters is predicted to oscillate as a function of the photon wavenumber with a frequency determined by the diameter of the cluster. The oscillations and other principal features of the photo cross section can be worked out analytically using semiclassical techniques. An accurate numerical calculation with different cluster potentials confirms these results qualitatively. Quantitative details depend sensitively on the actual potential. Hence, properties of the true cluster potential can be inferred from the experimental cross section. This might turn out to be useful for improving theoretical cluster potentials.

PACS: 36.40 + d; 32.80.Fb; 03.65.Sq

1 Introduction

Interaction with laser light has proved to be a sensitive tool to probe properties of clusters. Of recent interest are photoabsorption spectra in the energy window where the collective resonances in clusters occur [1] and photoionization around the threshold energy to determine the ionization potential as a function of the number of constituents in a cluster [2–6]. Experimental photoionization spectra for higher photon energies than a few eV (which is typically sufficient to ionize the cluster) have not yet been obtained. However, with the new synchrotron facilities such experiments become feasible.

Similarly, theoretical studies of photoionization have been limited to a few eV above the threshold [7, 8]. The theoretical description of photoionization of clusters – although fundamentally very simple and straightforward – poses some problems which are conceptually hard to overcome. They are related to the theoretical description of large alkali clusters which is based on the jellium approximation, i.e. a free electron gas consisting of the valence electrons of each atom and a homogeneous positively charged background of the ionic cores. Within the jellium model, density functional theory (DFT) and approximations of the exchange and correlation effects of the electron gas such as the local density approximation (LDA) can be used to calculate ground state properties of the clusters [3, 4]. The DFT generates an effective potential in which single particle states live.

To calculate dynamical processes with this potential such as photoionization is problematic for three reasons. Firstly, the single particle wave functions are not the actual electron wavefunctions which are necessary to calculate the dipole matrix element for the photo cross section. Secondly, the outgoing continuum wavefunction of the ionized electron feels the potential of the ionized, i.e. positively charged cluster so that the relevant potential should have a long range Coulomb tail. While the effective potential might be corrected in a reasonable way for this obvious long range behavior the more subtle long range features such as polarization of the cluster are also not very well represented by the effective potential which has been obtained from calculating the ground state (whose wavefunction is of course not sensitive to long range effects). Thirdly, the electromagnetic field of the light waves influences the loosely bound electrons, i.e. the charge density of the valence electrons. This results in a screening of the field and in an effective interaction of the valence electrons with the field which differs substantially from the dipole operator acting on a single electron in atoms or molecules as pointed out in [7].

The first issue is an obstacle which also applies to photoexcitation of clusters. However, there it has turned out that the naive approach of interpreting the single particle wavefunctions as the true electron wavefunctions works surprisingly well. The description of single electron excitations and collective plasmon excitations relies ultimately on the single particle spectrum supplied by various DFT methods [9].

The problem of the long range behavior could be partially avoided by considering photodetachment where the ionized cluster is neutral. Also, in this case, a refined theoretical approach, the time-dependent optimized potential method, yields accurate electron affinities [10] and one can hope that the long range properties of the effective

potential are realistically described. Hence, given the aforementioned problems, it seems to be most promising to calculate photodetachment. However, the goal of the present study is more explorative: To see which information about cluster properties can be extracted from the photoionization cross section and to examine *if* and *how* the cross section of large clusters is sensitive to details of the wavefunction and the potential. For this question we will not rely on the special advantages of photodetachment but study a more common case. We will consider ionization of a spherically symmetric neutral cluster whose effective potential does not change during the process of photoionization described within the usual single electron dipole approximation.

The last assumption seems to be in conflict with the shielding of the field as mentioned above. However, this effect is most pronounced for low photon energies where also other collective effects are to be expected. For higher photon frequencies the charge cloud of valence electrons can no longer follow the rapid change of the field and the shielding decreases. This behavior is confirmed in [7] where it is found that for higher photon energies (roughly 2.5 times the frequency of the classical Mie resonance which corresponds to about 10 eV) the ionization cross sections calculated with and without the shielding effect merge together. The calculation in [7] has been carried out up to these energies and we will consider photon energies larger than about 10 eV where the normal dipole approximation should be valid and collective effects are not to be expected. Towards high energies the range of validity of our study is limited by the onset of ionization of core electrons from single atoms in the cluster (about 40 eV for Na_N clusters).

The paper is organized as follows: in Sect. 2 we introduce three different models for cluster potentials and describe briefly how the photo cross section is formulated. The results of our numerical calculation are presented in Sect. 3, emphasizing the significant features of the photo cross section. In Sect. 4 we calculate the photo cross section analytically within a semiclassical approximation. Thereby, the functional dependence of the photo cross section on the photon energy is elucidated. Most importantly, we can show how the cluster size can be deduced from the photo cross section. Furthermore, we will discuss how the relevance of DFT potentials for photoionization can be checked. The paper ends with a conclusion in Sect. 5.

2 Photo cross section and effective potentials

2.1 The photo cross section

Within the dipole approximation the partial cross section σ_{fi} for photoionization of one electron from initial state Ψ_i to final state Ψ_f is given by

$$\sigma_{fi}(\omega) = \frac{(2\pi)^2 \alpha_F}{\omega} |\langle \Psi_f | \boldsymbol{De} | \Psi_i \rangle|^2, \tag{1}$$

where ω is the frequency of the ionizing photon which determines the energy of the outgoing electron through $E_f = \omega + E_i$, α_F is the fine structure constant, and $\boldsymbol{e}$ the polarization vector of the light. The dipole operator may be expressed in different gauges, namely in the length form ($\boldsymbol{D}_l = \omega \boldsymbol{r}$), the velocity form ($\boldsymbol{D}_v = -i\nabla_r$) or in the acceleration form ($\boldsymbol{D}_a = -i\nabla V(r)/\omega$). Throughout the paper we work in atomic units (a.u.) so that the cross section (1) is given in units of a_0^2. Under spherical symmetry of the system we can assign quantum numbers Elm for the final (continuum) state and $n'l'm'$ for the initial state where n describes the radial nodes and lm are the usual angular momentum quantum numbers. For unpolarized light the integration over the angles (θ, ϕ) can be performed analytically with the result [11]

$$\sigma_{El \leftarrow n'l'}(\omega) = \frac{(2\pi)^2 \alpha_F}{\omega} \frac{l_>}{2l'+1} |\langle \psi_{El}(r) | D | \psi_{n'l'}(r) \rangle_r|^2, \tag{2}$$

where $l_> = \max(l', l)$. Equation (2) includes the usual summation over all final magnetic states m_f and the average over the initial m_i states. Due to the dipole character of the incident light, the selection rules $\Delta l \equiv l - l' = \pm 1$ and $\Delta m = 0, \pm 1$ apply. The total cross section σ is the sum of the partial cross sections for all electrons in the cluster that take part in the process of photoionization at a given photon energy $\hbar\omega$. Electron $n'l'$ can be ionized if its binding energy $-E_{n'l'}$ is smaller than the photon energy. This leads to the formal expression for the total photo cross section (for more details see [11])

$$\sigma(\omega) = \sum_{l = l' \pm 1 \; \{n'l' \mid E_{n'l'} + \hbar\omega > 0\}} \sigma_{El \leftarrow n'l'}(\omega) \tag{3}$$

2.2 The cluster potential

To determine the wavefunctions $\psi_{n'l'}$ and ψ_{El} in (2) we need a potential which describes the dynamics of the valence electrons in the cluster. Such potentials are supplied by DFT calculations, an explicit example for the 34 valence electrons of the Na_{34} cluster from Ekardt [12] is shown in Fig. 1 (dashed line). As in nuclear physics, model potentials of the Woods–Saxon type (solid line in Fig. 1),

$$V_{WS}(r) = \frac{-V_0}{1 + \exp[(r - L)/a]}, \tag{4}$$

have been considered [13]. They have been justified by a good agreement of the energy spectrum with the numerical potential (in this case the DFT potential, see Table 1). However, as will be demonstrated, for dynamical quantities based on off-diagonal matrix elements (in contrast to diagonal matrix elements, e.g. energies) such as the dipole transition amplitude, the agreement among results from different cluster potentials is only qualitative. Quantitative details depend sensitively on the dynamics and that is on the wavefunctions which are different for each potential. This observation is confirmed by calculations with a modified Woods–Saxon potential (dotted-dashed line in Fig. 1),

$$V(r) = V_{WS}(r) - \frac{1}{r} \frac{1}{1 + \exp[(L - r)/b]}, \tag{5}$$

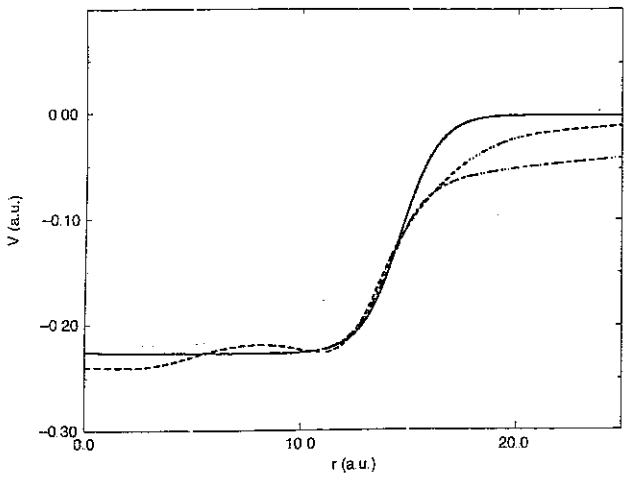

Fig. 1. Effective cluster potentials for Na_{34}. From a DFT calculation by Ekardt [12] (*dashed line*), from (4) with parameters $V_0 = 0.226$, $L = 14.478$ and $a = 0.9$ (*solid line*), from (5) with V_0 as before, $L = 13.930$, $a = 0.8$, $b = 0.7$ (*dotted-dashed line*)

Table 1. Electron energies (in a.u.) of bound states with the respective quantum numbers for the three different potentials

nl	Ekardt	Eq. 4	Eq. 5
1s	−0.20324	−0.20393	−0.20389
1p	−0.17904	−0.18156	−0.18154
1d	−0.15179	−0.15405	−0.15417
1f	−0.12053	−0.12193	−0.12243
2s	−0.14643	−0.14257	−0.14304

where the long range Coulombic part has been added without changing the bound state energies significantly (Table 1).

3 Numerical results

Following (2) it is straightforward to calculate the photo cross section numerically. For the effective one particle potential of Fig. 1 the bound state eigenfunctions are determined according to the shell model. That is for the spherically symmetric potential the shells, characterized by the quantum numbers nl, are filled successively beginning at small energies until the number of electrons required for the cluster size is reached. Each angular momentum level is $(2l + 1)$-fold degenerate. For each electron in a given shell nl there are two angular momentum states to which a dipole transition can occur according to $(\Delta l = \pm 1)$. To calculate the transition matrix elements we firstly compute the radial bound state and continuum wavefunction with the renormalized Numerov method [14]. The radial dipole matrix elements are then obtained by a simple quadrature. Once they are known the total photo cross section can be calculated according to (2).

The cross section is shown in Fig. 2 for the three different potentials of Fig. 1. We note that despite quantitative differences the three curves agree qualitatively with

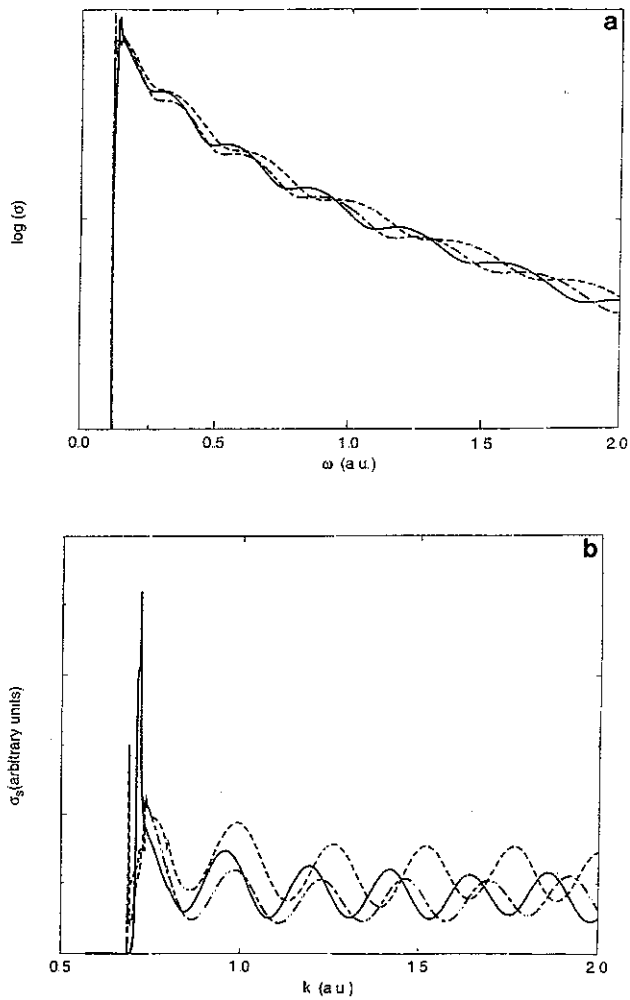

Fig. 2a, b. Total photo cross section as a function of the wavenumber for the potentials from Fig. 1, **a** in logarithmic scale as function of photon energy ω, **b** as a function of $k = \sqrt{2\omega + V_0}$ with the cross section scaled by the principal decrease of the yield, $\sigma_S(k) = k^7 \exp(2\pi a k)\sigma(k)/(1 + (ak)^2)$ with σ from (3)

respect to the following three features (see in particular Fig. 2b):

(i) The photo cross section decays exponentially as a function of the photon wavenumber $k \equiv \sqrt{2\hbar\omega + \delta}$ where δ is an energy offset to be determined.
(ii) The additional decrease is algebraic and proportional to $R(k)/\omega^{7/2}$, where $R(k)$ is a simple rational function whose precise form depends on the potential.
(iii) Superimposed on the monotonic decay an oscillation is observed with a constant frequency for larger wavenumbers k.

While *(i)* and *(ii)* are common features for photo cross sections [15] the superimposed oscillatory structure is unique for potentials with a sharp edge such as clusters. The frequency of the oscillation equals approximately the diameter of the cluster which can be seen by considering the Fourier transform of the cross section to length space (Fig. 3). The larger the k-range considered in the Fourier transform, the more pronounced the peak at the cluster

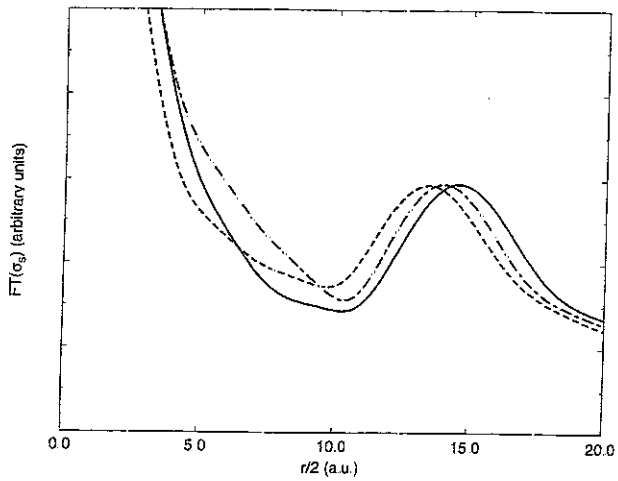

Fig. 3. Fourier transform of $\sigma_S(k)$ as a function of $r/2$ to show the connection to the cluster radius. The lines correspond to the potentials of Fig. 1

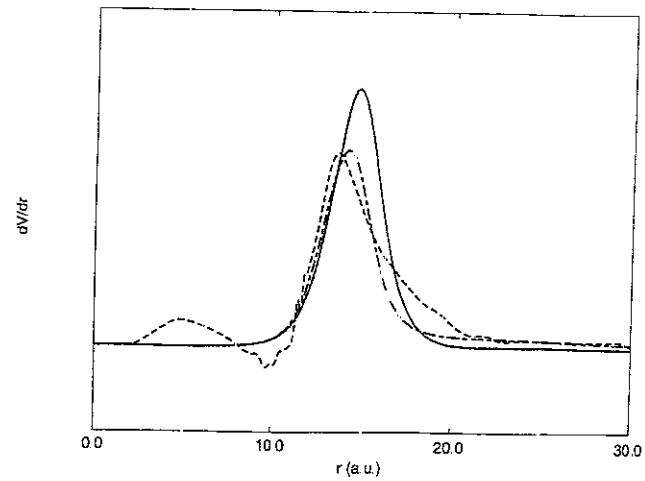

Fig. 4. Derivative of the three different potentials in Fig. 1 with respect to r. The coding of the lines is with respect to Fig. 1

diameter in length space. The Fourier transform may be used to determine the cluster radius directly from the photo cross section, provided a sufficiently large k-range can be taken into account. This opens the possibility for an *experimental determination of the cluster size from the photo cross section*. We will come back to this point in the next section. We also postpone the discussion of the obvious quantitative differences since their origin becomes more comprehensible when the analytic structure of the cross section is known.

4 Semiclassical analysis of the photoionization cross section

Using semiclassical WKB-wavefunctions and the method of stationary phase to evaluate the radial dipole matrix element (2) the photo cross section can be approximated analytically. Moreover, the evaluation of the integral is facilitated by the sharp edge of the cluster potential. Pictorially, this has the consequence that an electron, having absorbed a photon inside the cluster and leaving it with some velocity, will feel a sudden change in the potential passing the edge of the cluster. Formally, use of this effect can be made by expressing the dipole operator in the acceleration gauge as the derivative of the potential. The sudden change of the potential translates now to a dipole operator which is strongly peaked about the edge L of the potential (see Fig. 4). For the Woods–Saxon potential (4) it has the form

$$D(r) = \frac{1}{i\omega}\frac{V_0}{4a}\frac{1}{\cosh^2((r-L)/2a)} \equiv \frac{1}{i\omega}V' \tag{6}$$

Since the radial integral of (2) contains always a bound state wavefunction the classically allowed region for these states is most relevant. It is roughly given by the range of the potential well with depth $-V_0$. Hence, to obtain the major energy dependence of the cross section, it is sufficient to use WKB-wavefunctions where the potential has been approximated by $V(r) \approx -V_0$. Furthermore, the angular momentum dependence is weak and irrelevant for large photon energies ω. With these approximations we can write for the classical local wavenumber

$$k(r) = \sqrt{2E - 2V(r) - l(l+1)/r^2} \approx \sqrt{2E + 2V_0} \tag{7}$$

The WKB-functions have now the simple form [16]

$$\psi(r) \sim \frac{1}{\sqrt{k}}\cos(kr - \eta), \tag{8}$$

where the initial and final states are characterized by the respective energies E in (7) and by different phases η in (8). In the case of the initial state, η contains the quantization condition [16] while for the final continuum state η approximates the usual phase shift of the scattering wavefunction. The radial dipole integral reads

$$\langle \psi_f | D(r) | \psi_i \rangle \approx \frac{1}{2i}\,\mathrm{Re}(I_+ + I_-), \tag{9}$$

where

$$I_\pm = \frac{1}{\omega\sqrt{k_f k_i}}\int \mathrm{d}r\, e^{iS_\pm(r)} \tag{10}$$

with the phase

$$\begin{aligned} S_\pm(r) &= (k_f \pm k_i)r - (\eta_f \pm \eta_i) - i\ln V' \\ &\equiv k_\pm r - \eta_\pm - i\ln V' \end{aligned} \tag{11}$$

The integrals $I_\pm$ may be approximated by their value at the (complex) stationary phase point defined by

$$\frac{\mathrm{d}S_\pm}{\mathrm{d}r} = 0. \tag{12}$$

In the limit of large $k_\pm \equiv k$ we can solve (12) analytically for the Woods–Saxon potential (4) with the result

$$r_S = L + ia\pi \tag{13}$$

This leads finally to a total cross section whose dependence on the wavenumber of the photon can be expressed as (see (26) in the appendix)

$$\sigma(\omega) \propto \frac{R(k)}{\omega^{7/2}} e^{-\alpha k}(1 + \beta \cos(2kL - \gamma)), \tag{14}$$

where $k = (2\omega + \delta)^{1/2}$. The rational function $R(k)$ and hence the algebraic behavior even for large k depend on the potential. For the Woods–Saxon potential we obtain for $R(k)/\omega^{7/2} \sim \omega^{-5/2}$ while for a square well potential (which is obtained from (4) with an infinitely sharp edge, i.e. in the limit $a \to 0$) $R(k)$ is constant (see (26)–(28) in the appendix). Hence the algebraic behavior for high frequencies is $\omega^{-7/2}$ in this case. The constants α, β, γ and δ can be interpreted within the Woods–Saxon model potential in the following way (see appendix): α is proportional to a which controls how sharp the edge of the cluster potential is. The sharper the edge the slower the exponential decay of the cross section with k. In the limit of an infinitely sharp edge of the square well potential there is no exponential decay at all. The exponential decay is characteristic not only for the Woods–Saxon potential but also for DFT cluster potentials. Within our formalism it is easy to see that a functionally different behavior of the potential would also lead to a different dominant decay (e.g. for a Gaussian form of the derivative V' of the potential we find a Gaussian decay proportional to $\exp(-\alpha k^2)$ in the photo cross section).

The constants β and γ control the amplitude and phase of the oscillations and are in principle l-dependent. However, as argued in (8) this effect is negligible for larger k. The photon wavenumber k is theoretically expressed through the final energy E of the ionized electron and therefore differs for electrons from different shells. However, the differences are small and the theoretical expression can be linked to the more practical definition via $\hbar\omega = E - E_i$ in the following way: The highest occupied shells have the highest multiplicity and will contribute most to the ionization cross section. Their initial energy is for a neutral cluster roughly given by $E_i = -V_0/2$. Hence, $k^2 = 2E + 2V_0 \approx 2\omega + V_0$ so that $\delta \approx V_0$. This result may also be expressed as $\delta \approx 2E_b$ where E_b is the binding energy of the electron from the highest occupied shell.

Summarizing this analysis we see that details of the photo cross section depend quite sensitively on the form of the potential. Also the quantitative differences in the three cross sections (Figs. 2, 3) can now be explained from the form of the cluster potentials. The oscillations are not in phase and differ in amplitude for the three potentials since they generate different β and γ. A more robust quantity is the frequency of the oscillations linked to the cluster size. The small difference in the size L from the Fourier transform (Fig. 3) can be traced back to the location of the maximum of $V'(r)$ (Fig. 4) which enters the matrix element and the stationary phase condition (12). Despite the relatively good agreement of the energy spectrum among the three potentials (Table 1) the location of the maximum of V' is different for each of these potentials in a way which is consistent with the result for L from Fig. 3.

5 Conclusions

Using different model potentials for clusters we have investigated the photo ionization dynamics in terms of the total cross section. From numerical calculations as well as semiclassical analytical approximations we predict that the total photo cross section of spherically symmetric alkali metal clusters oscillates as a function of the photon wavenumber with a period that equals approximately the diameter of the cluster. This remains true as long as a deviation from the spherical shape can be described perturbatively which is the case for larger clusters.

Hence, it should be possible to determine the cluster radius experimentally from the Fourier transform of the photo cross section. On the other hand, the analysis of the features of the photo cross section reveals a sensitive dependence on the form of the potential. Such information may be extracted from future experiments and could be used to improve cluster potentials.

We would like to thank J.S. Briggs, C. Ellert and H. Haberland for helpful discussions. This work has been supported by the Deutsche Forschungsgemeinschaft within the SFB 276.

Appendix

The integral (10) can be evaluated by stationary phase in the following way

$$\int dr \exp(iS(r)) \approx \frac{\sqrt{2\pi i}}{|S''(r_S)|^{1/2}} \exp(iS(r_S)), \tag{15}$$

where r_S fulfills the condition

$$\frac{d}{dr} S(r_S) = 0, \tag{16}$$

i.e. r_S is the complex stationary point of the phase (11). For further reference we give the derivatives of the potential (4) with $y = (r - L)/(2a)$

$$V'(r) = \frac{V_0}{4a} \frac{1}{\cosh^2 y} \tag{17}$$

$$V''(r) = -\frac{V'(r)}{a} \tanh y$$

$$V'''(r) = -\frac{V'(r)}{2a^2}(1 - 3\tanh^2 y)$$

The stationary phase condition (16) leads to

$$ik_\pm = \left(-\frac{V''}{V'}\right) = \frac{1}{a} \tanh y \tag{18}$$

which is equivalent to

$$r_{S\pm} = L + 2ia \operatorname{atan}(ak_\pm). \tag{19}$$

Hence, the integral (10) has in stationary phase approximation the value

$$I_{\pm} = \frac{V_0\sqrt{\pi}}{2\omega\sqrt{k_i}}\sqrt{\frac{1+a^2k_{\pm}^2}{k_f}}\exp(ik_{\pm}L - i\eta_{\pm} - 2ak_{\pm}\,\mathrm{atan}(ak_{\pm})), \tag{20}$$

where the identity

$$\frac{1}{\cosh^2(i\mathrm{atan}\,x)} = (1+x^2) \tag{21}$$

has been used. Recalling the radial dipole matrix element from (9)

$$\langle\psi_f|D(r)|\psi_i\rangle \approx \frac{1}{2i}\,\mathrm{Re}(I_+ + I_-), \tag{22}$$

we get

$$\begin{aligned}|\langle\psi_f|D(r)|\psi_i\rangle|^2 &\approx \frac{C^2}{\omega^2 k_f}\exp(-4ak_f\mathrm{atan}(ak_{\pm}))\,[((A+B)^2\cos^2K_i \\ &+ (A-B)^2\sin^2K_i) + ((A+B)^2\cos^2K_i \\ &- (A-B)^2\sin^2K_i)\cos(2k_fL - 2\eta_f) \\ &+ ((A^2-B^2)\sin 2K_i)\sin(2k_fL - 2\eta_f)],\end{aligned} \tag{23}$$

with the abbreviations

$$K_i = k_iL - \eta_i \tag{24}$$

$$C = \frac{V_0}{4}\sqrt{\frac{\pi}{k_i}}$$

$$A = \sqrt{1+a^2k_+^2}\,\exp(-a2k_i\mathrm{atan}(ak_{\pm}))$$

$$B = \sqrt{1+a^2k_-^2}\,\exp(a2k_i\mathrm{atan}(ak_{\pm}))$$

For large $k_f \equiv k$ the approximations

$$k_+ \approx k_- \approx k \tag{25}$$

$$\mathrm{atan}(ak_{\pm}) \approx \frac{\pi}{2}$$

are valid. The total cross section (2) may then be written in the form (see (14))

$$\sigma(\omega) \approx D\,\frac{R(k)}{\omega^{7/2}}\exp(-2a\pi k)(1+\beta\cos(2kL-\gamma)), \tag{26}$$

where

$$R(k) = (1+a^2k^2)\frac{\sqrt{\omega}}{k} \tag{27}$$

$$D = \frac{V_0^2\pi^3\alpha_F}{2k_i}\,\frac{l_>}{2l'+1}\,(\cosh^2(a\pi k_i)\cos^2K_i + \sinh^2(a\pi k_i)\sin^2K_i)$$

$$\beta = \frac{\cosh^2(a\pi k_i)\cos^2K_i - \sinh^2(a\pi k_i)\sin^2K_i + \frac{1}{2}\sinh(2a\pi k_i)\sin 2K_i}{\cosh^2(a\pi k_i)\cos^2K_i + \sinh^2(a\pi k_i)\sin^2K_i}$$

$$\gamma = 2\eta_f + \mathrm{atan}\left(\frac{\frac{1}{2}\sinh(2a\pi k_i)\sin 2K_i}{\cosh^2(a\pi k_i)\cos^2K_i - \sinh^2(a\pi k_i)\sin^2K_i}\right)$$

Note that in the limit $a \to 0$ the Woods–Saxon potential approaches a square well. In this case (26) simplifies for large k to

$$\sigma(\omega) \approx \frac{1}{\omega^{7/2}}\,\frac{V_0^2\cos^2K_i\pi^3\alpha_F}{\sqrt{8}k_i}\,\frac{l_>}{2l'+1}(1+\cos(2kL-2\eta_f)) \tag{28}$$

as can be seen from (27).

References

1. Bréchignac, C., Connerade, J.P.: J. Phys. B **27**, 3795 (1994)
2. Saunders, W.A., Clemenger, K., deHeer, W.A., Knight, W.D.: Phys. Rev. B **32**, 1366 (1985)
3. deHeer, W.A.: Rev. Mod. Phys. **65**, 611 (1993)
4. Brack, M.: Rev. Mod. Phys **65**, 677 (1993)
5. Haberland, H.: Clusters of atoms and molecules. Berlin, Heidelberg, New York: Springer 1994
6. Bonačič-Koutecký, V., Fantucci, P., Koutecky, J.: Chem. Rev. **91**, 1035 (1991)
7. Ekardt, W.: Phys. Rev. B **65**, 6360 (1985)
8. Wästberg, B., Rosen, A.: Z. Phys. D **18**, 267 (1991)
9. Yannouleas, C., Vigezzi, E., Broglia, R.A.: Phys. Rev. B **47**, 9849 (1993)
10. Gross, E.K.U.: Private communication 1995
11. Friedrich, H.: Theoretische Atomphysik. Berlin, Heidelberg, New York: Springer 1990
12. Ekardt, W.: Phys. Rev. B **29**, 1558 (1984)
13. Nishioka, H., Hansen, K., Mottelson, B.R.: Phys. Rev. B **42**, 9377 (1990)
14. Johnson, B.R.: J. Chem. Phys. **67**, 4088 (1977)
15. Rost, J.M.: J. Phys. B **28**, L601 (1995)
16. Schiff, L.I.: Quantum mechanics. Singapore: McGraw-Hill 1968